Available *online* at : http://jnte.ft.unand.ac.id/

Jurnal Nasional Teknik Elektro

| ISSN (Print) 2302-2949 | ISSN (Online) 2407-7267 |

Equilibrium Control of Robot Arm Tip Mounted on a Transfer Coaxial Two-Wheel Robot

Toshiharu Yasui[1], Minoru Sasaki[1], Kojiro Matsushita[1], Joseph Muguro[1, 2], Waweru Njeri[1, 2], Titus Mulembo[1, 2]*

[1] *Department of Mechanical Engineering, Gifu University, 1-1 Yanagido, Gifu City, 501-1193*

[2] *Electrical and Electronics Department, Dedan Kimathi University of Technology, Nyeri, Kenya*

ARTICLE INFORMATION

Received: June 16, 2023
Revised: July 06, 2023
Accepted: July 06, 2023
Available online: July 31, 2023

KEYWORDS

Coaxial Two-wheel Robot, Equilibrium control, LQ, LQI Control

CORRESPONDENCE

E-mail: sasaki@gifu-u.ac.jp

A B S T R A C T

Japan has continued to experience population decline which adversely affect working-age group (15-64 years). As a remedy to this social issue, advancements in robotics and human-machine cooperation is proposed to make up for the declining labor force. To this end, design of robots which can work in constrained (indoor) workspace is desirable. A coaxial two-wheeled robot with an appended robot arm aimed at transporting objects is proposed in this paper. The robot is designed with center of gravity below the axle to make it statically stable at rest. It is combined with a robot arm with two links, two degrees of freedom. The goal is to maintain equilibrium of the arm tip during motion with the robot-arm is inclined at 0-, 3-, and 120-degree. In this study, simulations to combine a stable coaxial two-wheel robot with the robot arm is performed to confirm the effectiveness of the designed LQ, and LQI controller. From the results, all the controllers are able to maintain the robot-arm tip at 0-degrees. For 120-degrees, LQI performs better than LQ controller in stabilizing the rotation speed of the wheels by 1.7 seconds. In the future, the proposed controller model will be incorporated in the actual robot to confirm the performance for object transportation.

INTRODUCTION

For the last decade, Japan has been experiencing a population decline which adversely affect working-age group (15-64 years) [1]. This comes in manifestation of increased population of elderly, so called "super-aging" society as well as a declining birthrate [2]. According to 2019 population statistics, it is estimated that more than 28.4% of the total population is above the age of 65 years [3]. Consequently, the labor force (number of employees) is adversely affected. Therefore, the shortage of personnel has become a problem in various industries such as foods and drinks, homecare, and manufacturing industries to name a few. There is an option to raise wages as an incentive to increase personnel, but it is impractical in the long run due to the high cost of living in the country. The alternative is to employ technological advancements in robots and human-machine cooperation to make up for the lack of personnel. In this case, the robot assist human activities and/or replaces a worker in performing a piece of work [4]–[8].

Considering the food and drink industry, when serving food to consumers in restaurants, the operations have been automated using conveyor belts by restaurants in Japan. A challenge with this approach is that, with large-scale operations, the installation work is costly and rigid allowing for no alterations once setup. The alternative approach is automation with a focus on human-machine cooperation, to have a robot that can be reprogrammed and cooperate with humans in a typical working environment [6]. In this case, a mobile robot to carry objects, with minimal requirements that can operate in large-scale equipment installation is needed.

Currently, mobile robots are being introduced for the purpose of transporting objects at manufacturing sites such as factories and warehouses [3]. However, the size of robots used in factories is large, making them unsuitable for indoor work such as in restaurants. Additionally, factories are structured with demarked areas for robot operation and safety lines. On the contrary, a typical restaurant does not have such large spaces to demarcate regions.

To this end, biped and coaxial two-wheeled robots have been theorized to overcome such challenges [9], [10]. The robot features a small form factor, low power, collision sensing, to name a few advantages of this robots. This makes them ideal for indoor environments. In addition, safety is indispensable in space where humans live. For ease of control, coaxial two-wheeled robot is convenient for the environment as it has two powered wheels as compared to a biped that have multiple powered joints

https://doi.org/10.25077/jnte.v12n2.1106.2023

for locomotion alone. To this end, the research focused on the two-wheeled coaxial robot usable in an indoor environment.

Two-wheeled inverted pendulum (TWIP) robot can be broadly categorized based on the structural construction. The conventional model are the inverted pendulum type robots [11]–[13]. The TWIP robots are structurally unstable and need constant control to maintain balance. That is, TWIPs use the upper body to obtain and maintain dynamic balance based on the zero-moment point. Therefore, it is necessary to constantly control the robot to prevent it from falling [14]. The control of such system is highly nonlinear and is often linearized at equilibrium points. IP robots need to move the wheels as well as tilt the upper body in case of a disturbance. Huge disturbances will require actuation of motors and wheel movement than the system is incapable of producing and thus the TWIP robot is unable to recover from disturbances [15], [16]. In addition, the system is inherently dependent on the controller, that is, if an abnormality occurs in any one of the control systems such as the power supply, sensor, or actuator, there is a risk of falling.

The alternative to conventional TWIP is the use of stable coaxial wheel. In this case, the center of gravity of the IP type is set lower than the axle position, so that it is stabilized by physical force even when there is no power supply. This structure proposed in [17] was shown to be in stable in flat surfaces but faced challenges in unstable in rough terrains and elevations, similar to conventional IP robots. A remedy to this challenge was introduced in [11], [18] by dividing the vehicle body vertically such that each of the link can be controlled individually. In this research, the modified, statically stable model of TWIP is adopted.

Several control schemes have been proposed to regulate the operations of TWIP. PID is the most common as it does not require the construction of a model, just a fine tuning of the control parameters in a trial-error based approach or experience. The challenge with PID approach is that it does not account for disturbances. Another approach is on decoupled state space controllers for pitch and yaw movements. Linear quadratic regulator (LQR), fuzzy logic, neural networks among others have also been proposed. On the model-based strategies, Newtonian mechanics, Lagrangian formulation, and Kane's method have been applied. For this research, the system of equations representing the dynamics of the two-wheeled system will be derived using lagrangian formulation.

It is prudent to note that most of this research are geared towards the stabilization of the TWIP robot towards a self-balancing mode of operation. The present research however is targeting the control of a TWIP robot as well as the tip of a manipulator arm affixed to it. As such, we found few research inquiries focusing on this area. A research in [19] conducted a triple inverted pendulum control scheme which is closest to the present study. However, the proposal utilized a four-legged mobile robot which has better stability as compared to two-wheeled robot. Further, the authors used camera and neural networks to optimize control of inverted pendulums.

In this research, we aim to realize an object-carrying robot system by combining a coaxial two-wheeled robot with a static and stable inverted pendulum structure whose center of gravity is lower than the axle with an attached robot arm. This attached arm is intended to be utilized in balancing objects in a restaurant for example a tray of plates. As such, the arm does not exhibit large movement or swinging motions like a typical robot manipulator. Hence, the purpose of the research is to stabilize the arm around the vertical equilibrium point. At this point, the dynamics of the arm is not non-linear and can be sufficiently handled by approximate linearization.

Since the stable coaxial two-wheeled robot tilts when moving, stable object movement is difficult. Therefore, in this study, we aim at stable object transportation by combining a TWIP robot with a robot arm with two links and two degrees of freedom. The study investigates the tip equilibrium during motion both in simulation and experimentally and compares the performance using different control strategies.

ROBOT DESIGN

In this section, we will model the robot that is the control target required for simulation, determine the control method, and design the controller. The actual robot used in the study is shown in Figure 1.

Figure 1. The coaxial robot with appended manipulator robot arm.

Parameter Definition

The robot to be controlled consists of four elements: vehicle body 1, vehicle body 2, vehicle body 3 and wheels. The wheels and the vehicle body 2 are driven by the motor attached to the vehicle body 1, and the vehicle body 3 is driven by the motor attached to the vehicle body 2. θ_1 is the posture angle of the vehicle body 1, θ_2 is the posture angle of the vehicle body 2 with respect to the vehicle body 1, θ_3 is the posture angle of the vehicle body 3 with respect to the vehicle body 2, and φ is the rotation angle of the wheels. The posture angle of the vehicle body 2 is represented by $\theta_1 + \theta_2$, and the posture angle of the body 3 is represented by $\theta_1 + \theta_2 + \theta_3$. The parameter subscripts p_1, p_2, p_3 and c represent vehicle body 1, vehicle body 2, vehicle body 3, and wheels, respectively. The equations (1) - (3) gives the position derivation of position for body 1, 2 and 3, respectively. Appendix A show the equations and derivation for position and velocity of the robot bodies used in the study.

A conceptual diagram of the model is shown in Figure 2, and all parameters required for the model are tabulated as shown in Table 1. Motors are attached to the left and right wheels respectively to make a turning motion, but only linear motion is the subject of this study.

https://doi.org/10.25077/jnte.v12n2.1106.2023

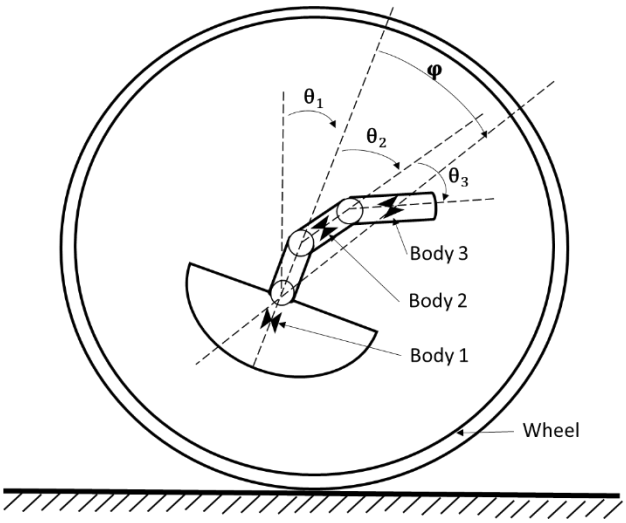

Figure 2. Coaxial two-wheel robot with pedestal body and manipulator arm structural illustration (not to scale).

$$\begin{bmatrix} x \\ y \end{bmatrix} = \begin{bmatrix} r(\varphi + \theta_1) \\ r \end{bmatrix} \quad (1)$$

$$\begin{bmatrix} x \\ y \end{bmatrix} = \begin{bmatrix} r(\varphi + \theta_1) - l_1 \sin\theta_1 \\ r - l_1 \cos\theta_1 \end{bmatrix} \quad (2)$$

$$\begin{bmatrix} x \\ y \end{bmatrix} = \begin{bmatrix} r(\varphi + \theta_1) + d\sin\theta_1 + l_2 \sin(\theta_1 + \theta_2) \\ r + d\cos\theta_1 + l_2 \cos(\theta_1 + \theta_2) \end{bmatrix} \quad (3)$$

$$\begin{bmatrix} x \\ y \end{bmatrix} = \begin{bmatrix} r(\varphi + \theta_1) + d\sin\theta_1 + L_2 \sin(\theta_1 + \theta_2) + \cdots \\ r + d\cos\theta_1 + L_2 \cos(\theta_1 + \theta_2) + \cdots \\ \cdots \quad l_3 \sin(\theta_1 + \theta_2 + \theta_3) \\ \cdots \quad l_3 \cos(\theta_1 + \theta_2 + \theta_3) \end{bmatrix} \quad (4)$$

Table 1. Parameter notations of coaxial robot

	Body1	Body2	Body3	Wheel
Mass	M_{p1}	M_{p2}	M_{p3}	M_c
Moment of Inertia	J_{p1}	J_{p2}	J_{p3}	J_c
Center of gravity distance	l_1	l_2	l_3	-
Length	-	L_2	-	-
Wheel radius	-	-	-	r
Coefficient of friction	C_{p1}	C_{p2}	C_{p3}	C_c
Motor coefficient	-	a_{p2}	a_{p3}	a_{pc}

Equation of Motion

The robot's equation of motion is derived from the Lagrangian equation of motion as shown in (5).

$$\frac{d}{dt}\left(\frac{\partial L}{\partial \dot{q}_i}\right) - \frac{\partial L}{\partial q_i} + \frac{\partial F}{\partial \dot{q}_i} = \tau_i \quad (5)$$

Where L, the Lagrangian function, is the difference between kinetic energy (T = 0.5mv^2), and potential energy ($V = mgh$) during robot motion, i.e. $L = T - V$ as described in [20]. The Lagrangian equation above is dissipative, i.e. friction forces are in play. Dissipated energy, F in this case is related to friction force. q_i is the generalized coordinate while τ_i is the generated force in the direction of q_i.

For the model, the inputs to body 2, body 3 and wheel drive motors are defined as u_{p2}, u_{p3} and u_c, respectively. The gravitational acceleration is g. The equations of motion obtained by applying the Lagrangian equations of motion to (1) – (4) is shown in Appendix (B1), (B2), (B3), (B4) corresponding to body 1, body 2, body 3 and drive wheels, respectively.

Linearization and State Equations

The goal of the paper is to perform tip control during robot motion. As such, the robot operations near equilibrium is obtained by linearization. Linearization of (B1), (B2), (B3) and (B4) is performed by assuming that $\theta_1, \theta_2, \ \theta_3, \ \theta_1 + \theta_2, \ \theta_2 + \theta_3$ and $\theta_1 + \theta_2 + \theta_3$ are near 0. The variables that are linearized are as follows.

$sin\,\theta_1 \cong \theta_1, \quad cos\,\theta_1 \cong 1, \quad sin\,\theta_2 \cong \theta_2, \quad cos\,\theta_2 \cong 1, \ sin\,sin\,\theta_3 \cong \theta_3, \quad cos\,\theta_3 \cong 1, \quad sin\,(\theta_1 + \theta_2) \cong (\theta_1 + \theta_2), \ cos\,(\theta_1 + \theta_2) \cong 1, \quad sin\,(\theta_2 + \theta_3) \cong (\theta_2 + \theta_3), \quad cos\,(\theta_2 + \theta_3) \cong 1, \quad sin\,(\theta_1 + \theta_2 + \theta_3) \cong (\theta_1 + \theta_2 + \theta_3), \quad cos\,(\theta_1 + \theta_2 + \theta_3) \cong 1.$

$\dot{\theta}_1^2 \cong 0, \quad (\dot{\theta}_1 + \dot{\theta}_2)^2 \cong 0, \quad (\dot{\theta}_1 + \dot{\theta}_2 + \dot{\theta}_3)^2 \cong 0, \quad \dot{\theta}_1\dot{\theta}_2 \cong 0$, $\dot{\theta}_1(\dot{\theta}_1 + \dot{\theta}_2) \cong 0, \quad \dot{\theta}_1(\dot{\theta}_2 + \dot{\theta}_3) \cong 0, \quad (\dot{\theta}_1 + \dot{\theta}_2)\dot{\theta}_2 \cong 0, \ (\dot{\theta}_1 + \dot{\theta}_2)\dot{\theta}_3 \cong 0, \quad \dot{\theta}_1(\dot{\theta}_1 + \dot{\theta}_2 + \dot{\theta}_3) \cong 0, \quad (\dot{\theta}_1 + \dot{\theta}_2 + \dot{\theta}_3)\dot{\theta}_3 \cong 0, \quad (\dot{\theta}_1 + \dot{\theta}_2 + \dot{\theta}_3)(\dot{\theta}_2 + \dot{\theta}_3) \cong 0.$

The linearized operation with the above conditions leads to a new set of equation shown in Appendix (C1), (C2), (C3), and (C4). The derived equations are represented in state space format with state variables x and input variables u as defined in (6) and (7).

$$\mathrm{x} = \begin{bmatrix} \theta_1 \\ \theta_1 + \theta_2 \\ \theta_1 + \theta_2 + \theta_3 \\ \varphi \\ \dot{\theta}_1 \\ \dot{\theta}_1 + \dot{\theta}_2 \\ \dot{\theta}_1 + \dot{\theta}_2 + \dot{\theta}_3 \\ \dot{\varphi} \end{bmatrix} \quad (6)$$

$$\boldsymbol{u} = [\boldsymbol{u_{p2}}\ \boldsymbol{u_{p3}}\ \boldsymbol{u_c}]^{\boldsymbol{T}} \quad (7)$$

Here, the physical meaning of each variable is as follows.

θ_1	:	Attitude angle of body 1
$\theta_1 + \theta_2$	:	Attitude angle of body 2
$\theta_1 + \theta_2 + \theta_3$	:	Attitude angle of body 3
φ	:	Wheel rotation angle
$\dot{\theta}_1$	:	Attitude angular velocity of body 1
$\dot{\theta}_1 + \dot{\theta}_2$	:	Attitude angular velocity of body 2
$\dot{\theta}_1 + \dot{\theta}_2 + \dot{\theta}_3$	:	Attitude angular velocity of body 3
$\dot{\varphi}$	:	Wheel rotation speed
u_{p2}	:	Input to the body 2 drive motor
u_{p3}	:	Input to the body 3 drive motor
u_c	:	Input to wheel drive motor

In addition, the coefficients for each state variable are summarized as follows.

$$\begin{aligned}
a_{11} &= (M_{p1}+M_{p2}+M_{p3}+M_c)r^2 + M_{p1}l_1^2 - 2M_{p1}rl_1 \\
&\quad + M_{p2}d^2 + M_{p2}rl_2 + 2M_{p2}rd + M_{p2}dl_2 \\
&\quad + M_{p3}d^2 + M_{p3}rL_2 + M_{p3}rl_3 + 2M_{p3}rd \\
&\quad + M_{p3}dL_2 + M_{p3}dl_3 + J_{p1} + J_c \\
a_{12} &= M_{p2}l_2^2 + M_{p2}rl_2 + M_{p2}dl_2 + M_{p3}L_2^2 + M_{p3}rL_2 \\
&\quad + M_{p3}L_2l_3 + M_{p3}dL_2 + J_{p2} \\
a_{13} &= M_{p3}l_3^2 + M_{p3}rl_3 + M_{p3}L_2l_3 + M_{p3}dl_3 + J_{p3} \\
a_{14} &= (M_{p1}+M_{p2}+M_{p3}+M_c)r^2 - M_{p1}rl_1 + M_{p2}rl_2 \\
&\quad + M_{p2}rd + M_{p3}rL_2 + M_{p3}rl_3 + M_{p3}rd \\
&\quad + J_c \\
a_{21} &= M_{p2}rl_2 + M_{p2}dl_2 + M_{p3}rL_2 + M_{p3}rl_3 + M_{p3}dL_2 \\
&\quad + M_{p3}dl_3 \\
a_{22} &= M_{p2}l_2^2 + M_{p3}L_2^2 + M_{p3}L_2l_3 + J_{p2} \\
a_{23} &= M_{p3}l_3^2 + M_{p3}L_2l_3 + J_{p3} \\
a_{24} &= M_{p2}rl_2 + M_{p3}rL_2 + M_{p3}rl_3 \\
a_{31} &= M_{p3}rl_3 + M_{p3}dl_3 \\
a_{32} &= M_{p3}L_2l_3 \\
a_{33} &= M_{p3}l_3^2 + J_{p3} \\
a_{34} &= M_{p3}rl_3 \\
a_{41} &= (M_{p1}+M_{p2}+M_{p3}+M_c)r^2 - M_{p1}rl_1 + M_{p2}rd \\
&\quad + M_{p3}rd + J_c \\
a_{42} &= M_{p2}rl_2 + M_{p3}rL_2 \\
a_{43} &= M_{p3}rl_3 \\
a_{44} &= (M_{p1}+M_{p2}+M_{p3}+M_c)r^2 + J_c
\end{aligned}$$

From the above, the equation (8) is obtained.

$$\begin{cases} \dot{x} = Ax + Bu \\ y = Cx \end{cases} \qquad (\mathbf{8})$$

Where,

$$\boldsymbol{A} = \begin{bmatrix} \mathbf{0}_{4\times4} & \boldsymbol{I}_{4\times4} \\ -\boldsymbol{\alpha}^{-1}\boldsymbol{\gamma} & -\boldsymbol{\alpha}^{-1}\boldsymbol{\beta} \end{bmatrix}$$

$$\boldsymbol{B} = \begin{bmatrix} \mathbf{0}_{4\times4} \\ \boldsymbol{\alpha}^{-1}\boldsymbol{\delta} \end{bmatrix}$$

$$\boldsymbol{C} = [\boldsymbol{I}_{8\times8}]$$

$$\alpha = \begin{bmatrix} a_{11} & a_{12} & a_{13} & a_{14} \\ a_{21} & a_{22} & a_{23} & a_{24} \\ a_{31} & a_{32} & a_{33} & a_{34} \\ a_{41} & a_{42} & a_{43} & a_{44} \end{bmatrix}$$

$$\boldsymbol{\beta} = \begin{bmatrix} C_{p1} & 0 & 0 & 0 \\ -C_{p2} & C_{p2} & 0 & 0 \\ 0 & -C_{p3} & C_{p3} & 0 \\ 0 & 0 & 0 & C_c \end{bmatrix}$$

$$\boldsymbol{\gamma} = \begin{bmatrix} M_{p1}gl_1 - (M_{p2}d + M_{p3}d)g & -(M_{p2}l_2 + M_{p3}L_2)g & -M_{p3}gl_3 & 0 \\ 0 & -(M_{p2}l_2 + M_{p3}L_2)g & -M_{p3}gl_3 & 0 \\ 0 & 0 & -M_{p3}gl_3 & 0 \\ 0 & 0 & 0 & 0 \end{bmatrix}$$

$$\boldsymbol{\delta} = \begin{bmatrix} 0 & 0 & 0 \\ a_{p2} & 0 & 0 \\ 0 & a_{p3} & 0 \\ 0 & 0 & a_c \end{bmatrix}$$

Control Method

In this research, regulator controller is utilized. A regulator is a system that asymptotically returns to the equilibrium state when the state variable deviates from the equilibrium state (arbitrary initial state). Since the goal is to converge the angle of the robot arm tip (Body 3) to 0 [deg], regulator control was adopted.

Control using an optimal regulator (hereinafter referred to as LQ control) refers to control using state feedback. The block diagram is shown in Figure 3.

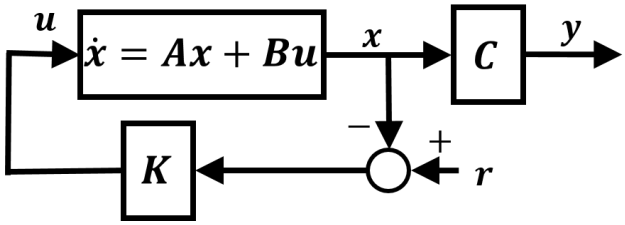

Figure 3. LQ controller.

This is a method in which an optimal regulator is considered whereby the state feedback gain K minimizes the performance index J to obtain the optimal control input u [21]. Here, the performance index J is as shown in (9), and the optimal control input u is equation (10). r is the target value.

$$J = \int_0^\infty (x^T Q x + u^T R u)\, dt \qquad (\mathbf{9})$$

$$u = K(r - x) \qquad (10)$$

$\boldsymbol{Q}$ is the output and $\boldsymbol{R}$ is the weight matrix for the input. The state feedback gain K that minimizes (9) is given by (11).

$$K = R^{-1}B^T P \qquad (11)$$

In this case, $\boldsymbol{P}$ is a positive definite symmetric solution that satisfies the Riccati equation shown in (12).

$$PA + A^T P - PBR^{-1}B^T P + Q = 0 \qquad (12)$$

From (10) and (11), the optimal control input u is expressed by (13).

$$u = R^{-1}B^T P(r - x) \qquad (13)$$

The weight matrix used for Q and R in the design is shown below. The optimal weight factor of feedback gains K' used is shown in table 3.

$$Q = diag(1{,}90{,}150{,}1{,}1{,}1{,}130{,}1)$$
$$R = diag(70{,}15{,}70)$$

IDENTIFICATION OF UNKNOWN PARAMETERS

In designing a controller, it is necessary to find various parameters of the robot. Weight and length are obtained by actual measurements while the moment of inertia is calculated from measured so obtained. However, the friction coefficient is an unknown parameter. Therefore, the friction coefficient is to be identified by experiments.

Madgwick filter was applied to measure the angle of each vehicle body in the unknown parameter identification experiment. The filter was proposed by S. Madgwick [22], which is applied to the values of the 3-axis acceleration and 3-axis gyro data acquired from the 6-axis motion sensor and used. Compared with the Kalman filter, Madgwick filter has been shown to achieves high speed of operations and an accuracy [23], [24].

Identification of Body 1 Friction Coefficient

The friction coefficient of the vehicle body 1 was obtained by measuring the initial value response of the posture angle of the

https://doi.org/10.25077/jnte.v12n2.1106.2023

robot body and comparing it with the simulation results. The altitude angle of the main body was inclined by 35 [deg] when the initial value response was measured. The experiment was conducted with the wheel drive motor, vehicle body 2 drive motor, and vehicle body 3 drive motor fixed. The equation used for the simulation is shown in (14).

$$\begin{aligned}\{&(M_{p1}+M_{p2}+M_{p3}+M_c)r^2+M_{p1}l_1^2-2M_{p1}rl_1+M_{p2}d^2\\&+2M_{p2}rl_2+2M_{p2}rd+2M_{p2}dl_2+M_{p3}d^2\\&+2M_{p3}rL_2+2M_{p3}rl_3+2M_{p3}rd\\&+2M_{p3}dL_2+2M_{p3}dl_3+J_{p1}+J_c+M_{p2}l_2^2\\&+M_{p3}L_2^2+2M_{p3}L_2l_3+J_{p2}+M_{p3}l_3^2\\&+J_{p3}\}\ddot{\theta}_1+\{C_{p1}\}\dot{\theta}_1\\&+\{M_{p1}gl_1-M_{p2}gl_2-M_{p2}gd\\&-M_{p3}gL_2-M_{p3}gl_3-M_{p3}gd\}\theta_1=0\end{aligned}\quad(14)$$

A comparison of simulated body 1 angles and experimental results is shown in Figure 4. The friction coefficient C_{p1} of body 1 was set to 0.045, while that of C_{p2} and C_{p3} of body 2 and 3, respectively, was set to 0.004.

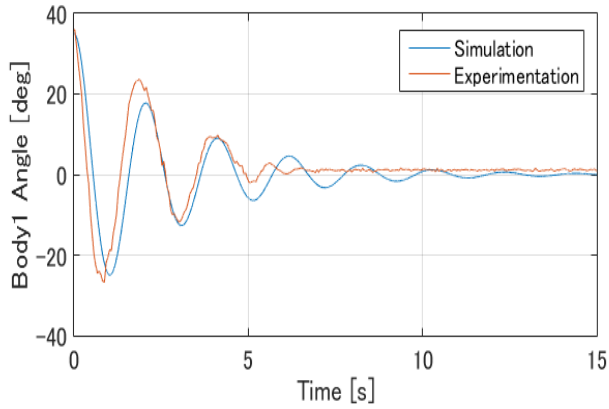

Figure 4. Body 1 Simulation and experiment comparison

Identification of Body 2 and 3 friction coefficients

The friction coefficient of vehicle body 2 was calculated by adding the input to vehicle body 2 drive motor, measuring the response, and comparing it with the simulation results. At this time, for safety, the robot body was turned upside down, and the wheel drive motor and the vehicle body 3 drive motor were fixed during experiment. Here, the equation used for the simulation is shown in (15).

$$\begin{aligned}\{&M_{p2}l_2^2+M_{p3}L_2^2+2M_{p3}L_2l_3+J_{p2}+M_{p3}l_3^2+J_{p3}\}\ddot{\theta}_2\\&+\{C_{p2}\}\dot{\theta}_2\\&+\{-M_{p2}gl_2-M_{p3}gL_2-M_{p3}gl_3\}\theta_2\\&=a_{p2}u_{p2}\end{aligned}\quad(15)$$

For body 3, the experiment was conducted with the wheel drive motor and the body 2 drive motor fixed. The equation used for the simulation is shown in (16).

$$\begin{aligned}\{&M_{p3}l_3^2+J_{p3}\}\ddot{\theta}_3+\{C_{p3}\}\dot{\theta}_3+\{-M_{p3}gl_3\}\theta_3\\&=a_{p3}u_{p3}\end{aligned}\quad(16)$$

The results are shown in Figure 5 and 6 below. In all this cases, there was good agreement between the simulation and the experiment pointing to appropriateness of the parameters adopted.

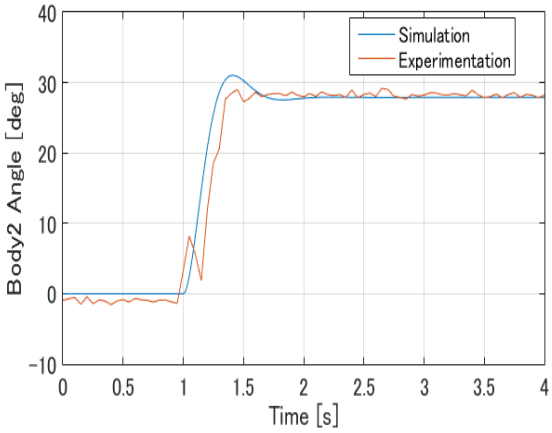

Figure 5. Body 2 simulation and experiment comparison

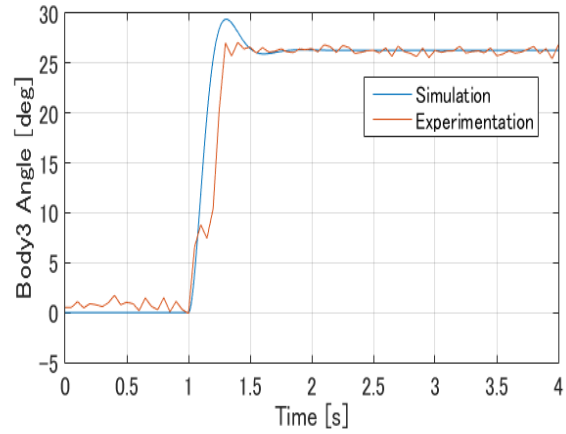

Figure 6. Body 3 simulation and experiment comparison

Identification of Wheel Friction Coefficient

The friction coefficient of the coaxial wheel axle was calculated by adding an input to the wheel drive system, measuring the response, and comparing it with the simulation results. At this time, the experiment was conducted with the vehicle body 2 and vehicle body 3 drive motor fixed. The equation used for the simulation is shown in (17).

$$\begin{aligned}\{&(M_{p1}+M_{p2}+M_{p3}+M_c)r^2+J_c\}\ddot{\varphi}+\{C_c\}\dot{\varphi}\\&=a_cu_c\end{aligned}\quad(17)$$

Figure 7 shows a comparison between the simulation results and the experimental results. The friction coefficient C_c of the axle was set to 0.430.

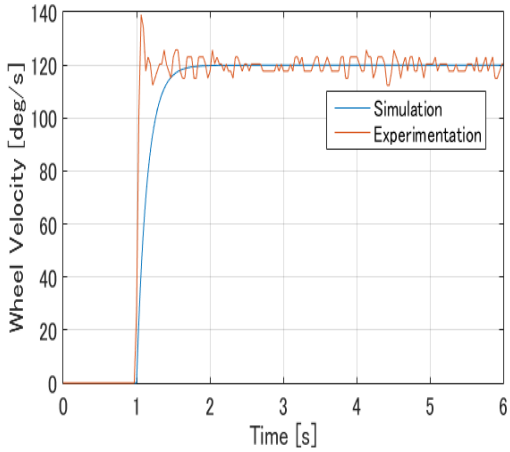

Fig. 7 Wheel simulation and experiment comparison

The above results point to a perfect agreement between experimentation and simulation of the robot motions. From this, the simulated results are thought to capture the necessary dynamics of the physical system. The simulation of different control schemes is investigated and reported in section below.

RESULTS

Simulation was performed using Simulink™ developed by Matlab® for model-based design. The simulation was performed for the purpose of verifying whether the posture angle $\theta_1 + \theta_2 + \theta_3$ of the body 3 remains 0° [degree] when the robot moves. The 3D model utilized in the simulation is shown Fig. 8 below.
The simulation was performed using a sampling time of 0.1 milliseconds with a square wave input control. The square wave was from t = 2 [s] to 7 [s] with respect to the wheel rotation speed $\dot{\varphi}$. The target value was set to 3° [deg / s] as described in the model equation (18).

$$\dot{\varphi} = \begin{cases} 0 & 0 \le t < 2,\ 7 \le t \\ 3 & 2 \le t < 7 \end{cases} \quad (18)$$

The values of the parameters used in the simulation are shown in Table 2. For verification, we compared LQR and PID methods in different forms to improve the performance of the proposed controller.

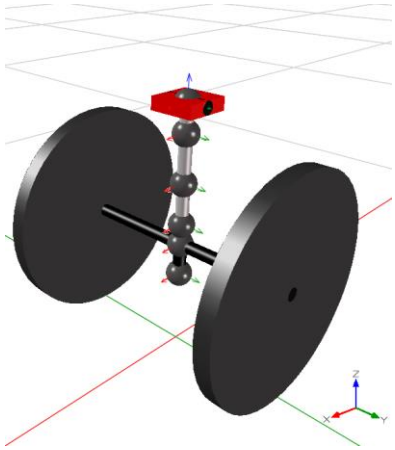

Figure 8. 3D Model.

Table 2. Parameters of the simulated coaxial robot

	Body 1	Body 2	Body 3	Wheel
Mass[kg]	1.3	0.15	0.15	0.77
Moment of inertia [kg・m^2]	0.0120	5.28×10^{-4}	1.52×10^{-4}	0.00866
Center of gravity distance[m]	0.080	0.055	0.030	-
Length [m]	-	0.7	-	-
Wheel radius[m]	-	-	-	0.15
Coefficient of friction	0.045	0.028	0.0040	0.43
Motor coefficientx [N・m]	-	1.5	1.5	6.0

Result of proposed model at a wheel inclination of 0° and 3°

Figure 9 shows the simulation results of the proposed model. From top to bottom, the attitude angle of the vehicle body 3, the attitude angle of the vehicle body 2, the attitude angle of the attitude angle of the vehicle body 1, and the rotational speed of the wheel $\dot{\varphi}$. From the simulation results, Body 3 maintains 0° and has succeeded in horizontal control. In addition, since the angles of Body1 and Body2 change symmetrically, the position of the center of gravity can be adjusted. However, the problem is that Body1 and Body2 sway greatly and Body3 sways vertically by adjusting the position of the center of gravity.
From this, additional controllers were sought that would counter the excessive swaying in the model. PD and LQ model results are described below. In this case, the wheel velocity is increased from 3°/second to 120°/second. The objective was still to maintain body 3 at a 0° equilibrium as previously.

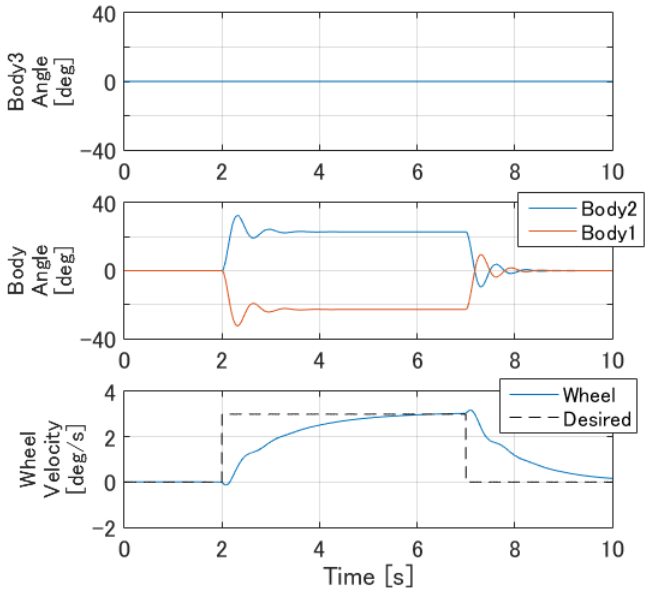

Figure 9. Performance of the proposed model

Tables should be typed and included in the main body of the article. The position of tables should be inserted in the text as close to the point of reference as possible. Ensure that any superscripts or asterisks are shown next to the relevant items and have corresponding explanations displayed as footnotes to the table, figure or plate.

LQ and PD Model Consideration

From Figure 10, looking at the posture angle of Body 3 at the top, it can be confirmed that both LQ control and PD control maintain 0° [deg]. However, the posture angles of Body 1 and Body 2 fluctuate more in PD control. Looking at the rotation speed of the wheel, PD control has overshoot, but the rising speed is faster, the target value is reached after 1 [s] and is stable after 2.5 [s]. On the other hand, in LQ control, the target value is reached and stable after 3 [s].

https://doi.org/10.25077/jnte.v12n2.1106.2023

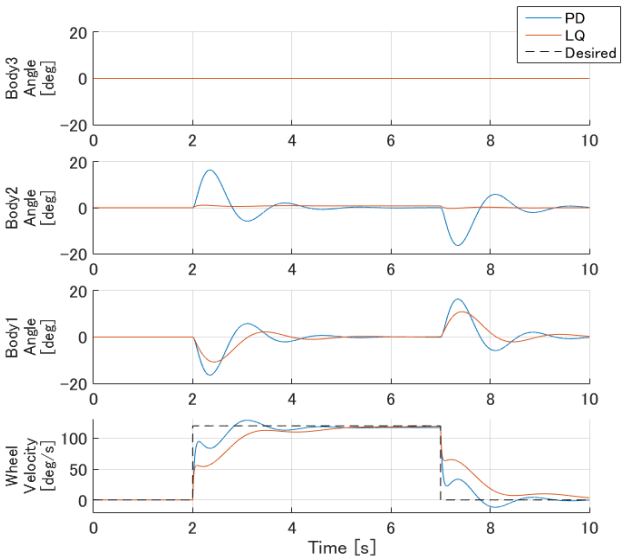

Figure 10. Comparison of PD with LQ model

To summarize the above, since Body 3 maintains 0°, either control method can be used for transporting an object. However, PD contains more instability due to swaying vertically. Furthermore, the maximum posture angle of each body is larger in PD control. Therefore, it is considered that LQ control is more suitable for transportation. The challenge with LQ control is that it has a poorer followability with the target value of the wheel rotation speed than the PD control.

As one of the improvement measures, it is possible to add an integrator to construct a servo system and introduce control using an integral type of optimum regulator (hereinafter referred to as LQI control)). It is considered that the target value tracking performance will be improved because the deviation that occurs is multiplied by the gain by integrating the error of the wheel rotation speed.

LQ and LQI controller at a wheel inclination of 0° and 120°

LQI control is performed using state feedback. In the simulation, the target value was set to 120° and the corresponding control equation shown in (19).

$$\dot{\varphi} = \begin{cases} 0 & 0 \le t < 2,\ 7 \le t \\ 120 & 2 \le t < 7 \end{cases} \quad (19)$$

Among the state variables, an integrator was added to the posture angle $\theta_1 + \theta_2 + \theta_3$ of the body 3 and the wheel rotation speed (φ) to compensate for the deviation. The reason for choosing the body 3 posture angle $\theta_1 + \theta_2 + \theta_3$ and the wheel rotation speed $\dot{\varphi}$ as compensation targets is that this study balances the body 3 posture angle $\theta_1 + \theta_2 + \theta_3$. In addition, this is to improve the trackability of the wheel rotation speed $\dot{\varphi}$ to the target value during movement.

The target values for the posture angle $\theta_1 + \theta_2 + \theta_3$ of the body 3 and the $\theta_1 + \theta_2 + \theta_3$ wheel rotation speed $\dot{\varphi}$ are $(\theta_1 + \theta_2 + \theta_3)_{ref}$ and $(\dot{\varphi})_{ref}$, respectively. The error integrated values obtained by taking the difference from the target value and integrating are $e_{(\theta_1+\theta_2+\theta_3)}$ and $e_{(\dot{\varphi})}$, respectively, and shown in equation (20) and (21).

$$e_{(\theta_1+\theta_2+\theta_3)} = \int_0^\infty [(\theta_1 + \theta_2 + \theta_3)_{ref} - (\theta_1 + \theta_2 + \theta_3)]\, dt \quad (20)$$

$$e_{(\dot{\varphi})} = \int_0^\infty [(\dot{\varphi})_{ref} - (\dot{\varphi})]\, dt \quad (21)$$

The error integration value is added to the state variable x in (10) to form an expanded state equation. The expanded state variable x_e is shown in equation (22) and the corresponding state equation is shown in (23).

$$\boldsymbol{x_e} = [\boldsymbol{x}\ e_{(\theta_1+\theta_2+\theta_3)}\ e_{(\dot{\varphi})}]^{\boldsymbol{T}} \quad (22)$$

$$\dot{\boldsymbol{x}}_{\boldsymbol{e}} = \boldsymbol{A_e x_e} + \boldsymbol{B_e u} + \boldsymbol{E_e h} \quad (23)$$

where

$$\boldsymbol{h} = [(\theta_1 + \theta_2 + \theta_3)_{ref}\ (\dot{\varphi})_{ref}]^T$$

$$\boldsymbol{A_e} = \begin{bmatrix} \boldsymbol{A} & \boldsymbol{0}_{8\times2} \\ -\boldsymbol{C_e} & \boldsymbol{0}_{2\times2} \end{bmatrix},\ \boldsymbol{B_e} = \begin{bmatrix} \boldsymbol{B} \\ \boldsymbol{0}_{2\times3} \end{bmatrix}$$

$$\boldsymbol{C_e} = \begin{bmatrix} 0 & 0 & 1 & 0 & 0 & 0 & 0 & 0 \\ 0 & 0 & 0 & 0 & 0 & 0 & 0 & 1 \end{bmatrix},\ \boldsymbol{E_e} = \begin{bmatrix} \boldsymbol{0}_{8\times2} \\ \boldsymbol{I}_{2\times2} \end{bmatrix}$$

Similar to LQ control, the state feedback gain K that minimizes the performance index shown in (24) is found from (23), and the optimal control input u shown in (25) is obtained.

$$J = \int_0^\infty (x_e{}^T Q x_e + u^T R u)\, dt \quad (24)$$

$$u = K(r - x) \quad (25)$$

The state feedback gain Ke that minimizes (24) is given by (25).

$$Ke = [K_1\ K_2] = R^{-1} B_e{}^T P \quad (25)$$

P is a positive definite symmetric solution that similarly satisfies the Riccati equation in (26).

$$PA_e + A_e{}^T P - PB_e R^{-1} B_e{}^T P + Q = 0 \quad (26)$$

From (25) and (26), the optimal control input u is represented by equation (27).

$$u = R^{-1} B_e{}^T P(r - x) \quad (27)$$

A controller was designed using the same parameters shown in Table 3. The weight matrix used for Q and R in the design is shown below. Table 5 shows the weight of feedback gains, Ke used.

$$Q = diag(25,10,110,1,1,1,160,1,130,1)$$

$$R = diag(20,55,80)$$

Fig. 11 shows a comparison of the simulation results of LQ control and LQI control using the weights described above.

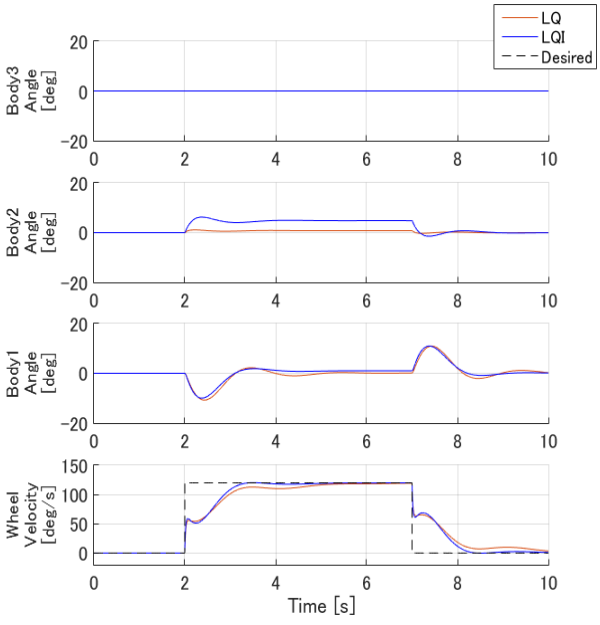

Fig. 11 Comparison of LQ and LQI controller.

By the LQI control that added an integrator to the posture angle of the Body 3 and the rotation speed of the wheels, the stability of the rotation speed of the wheels to the target value was increased by 1.7 [s] and the followability was improved.

Table 3. Weight factor of LQI gains (Ke')

-0.2360	-0.0286	-0.4327
0.8946	-0.0286	0.0112
-0.8573	2.6679	0.0214
0.0327	0.0042	0.0773
0.0978	0.0113	-0.0069
0.2135	0.0322	-0.0034
-0.5762	1.6674	0.0049
0.0924	0.0122	0.0931
0.5266	-1.5043	0.0002
-0.0327	-0.0042	-0.0773

DISCUSSIONS

The paper sought to investigate equilibrium control of the tip of a robot arm attached to pedestal TWIP robot. The intended use case being assisting in transporting objects placed on top of the robot arm in a restaurant setting. Thus, the tip is to be maintained at 0° irrespective of robot motion. To this end, the study performed experiments and simulations to verify performance with different TWIP robot at different inclinations, i.e., 0°, 3° and 120° as described in equation (18) and (19).

The study derived mathematical model of the TWIP robot with 2DoF robot arm using lagrangian equations to yield a state space model. Further, experimental data was collected both in simulation and physical robot to verify the agreement between the physical and identified model. the results had good agreement as shown in Fig. 4-7. This verified the simulation results obtained.

The performance of the modeled controller is shown in Fig. 9. From the results, Body3 maintains 0° and thus the study succeeded in horizontal control. In addition, since the angles of Body1 and Body2 change symmetrically, the position of the center of gravity can be adjusted. However, the problem is that Body1 and Body2 sway greatly and Body3 sways vertically by adjusting the position of the center of gravity. This is because the mass and moment of inertia of Body1 are much larger than those of Body2 and Body3, and the magnitude of the eigenvalues is significantly different.

To eliminate the huge oscillatory motions of body 2 and 3, we added PD, LQ and LQI controllers to enhance performance. From the results both LQ control and PD control maintain 0°. However, the posture angles of Body 1 and Body 2 fluctuate more in PD control compared to LQ. In contrast, LQ has a poorer followability with the target value of the wheel rotation speed than the PD controller.

As one of the improvement measures, LQI was introduced to improve target value tracking performance. From the results, posture angle of the Body 3 and the rotation speed of the wheels was better. The stability of the rotation speed of the wheels was improved by 1.7 seconds in LQI controller compared to LQ controller. From the above, the study achieved satisfactory equilibrium control with varying wheel velocities. Further, the proposed controllers aided the tracking performance in simulation results.

The present study faced a challenge in testing the developed controller in the actual robot. The testing required a high-performance data acquisition system to feedback information from the motor encoders which was missing in the current setup. The next step in the study will be upgrading the encoders for higher precision as well as integrating a high-performant data acquisition system to deploy the controller to the actual robot.

CONCLUSIONS

In this research, we aimed at equilibrium control of a coaxial robot with an appended robot arm with 2 links and 2 degrees of freedom. The proposed robot system is tasked with object transportation and hence equilibrium control of the robot arm tip is critical in a mobile state.

The equation of motion of the robot to be controlled was derived using the Lagrange equation of motion. The state equation was derived by determining the state variables and inputs. Several experiments were conducted to identify optimal parameters for the robot. A verification of the experimental values is done by simulation.

The proposed model design and simulation parameters are described, and comparison of the performance is compared between different control methodologies. In this case, PD, LQ and LQI control schemes are compared for equilibrium control of 0° at the tip with robot inclinations of 0°, 3° and 120°. From the results, we confirmed that the LQ and LQI controller designed for balanced control of the robot arm tip is effective.

As a future issue, it is necessary to incorporate the designed controller into the actual machine and confirm the control performance for object transportation.

ACKNOWLEDGMENT

This work is partially supported by Grants-in-aid for Promotion of Regional Industry-University-Government Collaboration from Cabinet Office, Japan.

REFERENCES

[1] "Decrease in working-age population," Cabinet Office Japan, 2017. [Online]. Available: https://www5.cao.go.jp/keizai-shimon/kaigi/minutes/2017/0125/shiryo_04-2-3.pdf. [Accessed: 29-May-2020].

[2] S. B. of Japan, "2015 Population Census," 2015. [Online]. Available: http://www.stat.go.jp/english/data/kokusei/2015/final_en/pdf/s01.pdf. [Accessed: 28-May-2020].

[3] Nippon.com, "Japan's Population Falls for Ninth Straight Year," nippon.com, Tokyo, 30-Apr-2020.

[4] P. W. Laksono, M. Sasaki, K. Matsushita, M. S. A. Bin Suhaimi, and J. Muguro, "Preliminary research of surface electromyogram (sEMG) signal analysis for robotic arm control," AIP Conf. Proc., vol. 2217, no. April, 2020, doi: 10.1063/5.0000542.

[5] N. W. Minoru Sasaki, Eita Kunii, Tatsuya Uda, Kojiro Matsushita, Joseph K. Muguro, Muhammad Syaiful Amri bin Suhaimi, "Construction of an Environmental Map including Road Surface Classification Based on a Coaxial Two-Wheeled Robot," J. Sustain. Res. Eng., vol. 5, no. 3, pp. 159–169, 2020.

 https://doi.org/10.25077/jnte.v12n2.1106.2023

[6] N. Abdul Malik, H. Yussof, F. A. Hanapiah, and S. J. Anne, "Human Robot Interaction (HRI) between a humanoid robot and children with Cerebral Palsy: Experimental framework and measure of engagement," in 2014 IEEE Conference on Biomedical Engineering and Sciences (IECBES), 2014, pp. 430–435, doi: 10.1109/IECBES.2014.7047536.

[7] N. Rudigkeit and M. Gebhard, "AMiCUS—a head motion-based interface for control of an assistive robot," Sensors (Switzerland), vol. 19, no. 12, 2019, doi: 10.3390/s19122836.

[8] M. Sasaki et al., "Robot control systems using bio-potential signals," AIP Conf. Proc., vol. 2217, no. April, 2020, doi: 10.1063/5.0000624.

[9] K. T. Kouho Sago, Yoshiyuki Noda, Kiyoaki Kakihara, "Vehicle Body Swing Suppression Control Considering Passenger's Body in Low-CV Parallel Two-wheel Vehicle," in Proceedings of the Japan Society of Mechanical Engineers Vol. 81, No. 824, 2015, p. 14.

[10] S. Ito, S. Nishio, M. Ino, R. Morita, K. Matsushita, and M. Sasaki, "Design and adaptive balance control of a biped robot with fewer actuators for slope walking," Mechatronics, vol. 49, pp. 56–66, 2018, doi: 10.1016/j.mechatronics.2017.11.007.

[11] L. C. GAO Xue-shan, DAI Fu-quan, "Two types of coaxial self-balancing robots," J. Cent. South Univ., vol. 20, p. 2981−2990, 2013, doi: 10.1007/s11771-013-1822-2.

[12] K. M. Goher, "A two-wheeled machine with a handling mechanism in two different directions," Robot. Biomimetics, vol. 3, no. 1, 2016, doi: 10.1186/s40638-016-0049-8.

[13] J. H. Park and B. K. Cho, "Development of a self-balancing robot with a control moment gyroscope," Int. J. Adv. Robot. Syst., vol. 15, no. 2, pp. 1–11, 2018, doi: 10.1177/1729881418770865.

[14] M. Khaled, A. Mohammed, M. S. Ibraheem, and R. Ali, "Balancing a Two Wheeled Robot," 2009.

[15] Z. Kausar, K. Stol, and N. Patel, Nonlinear control design using Lyapunov function for two-wheeled mobile robots. 2012.

[16] M. Sasaki et al., "Robust posture tracking control of stable coaxial two-wheeled AGV using the approximate inverse system and LMI," J. Appl. Sci. Eng. Technol. Dev., pp. 24–42, 2020, doi: 10.33803/jasetd.2020.4-1.3.

[17] M. Deng, A. Inoue, K. Sekiguchi, and L. Jiang, "Two-wheeled mobile robot motion control in dynamic environments," Robot. Comput. Integr. Manuf., vol. 26, no. 3, pp. 268–272, 2010, doi: 10.1016/j.rcim.2009.11.005.

[18] F. Dai, X. Gao, S. Jiang, W. Guo, and Y. Liu, "A two-wheeled inverted pendulum robot with friction compensation," Mechatronics, vol. 30, pp. 116–125, 2015, doi: 10.1016/j.mechatronics.2015.06.011.

[19] X. Huang, F. Wen, and Z. Wei, "Optimization of triple inverted pendulum control process based on motion vision," Eurasip J. Image Video Process., vol. 2018, no. 1, 2018, doi: 10.1186/s13640-018-0294-6.

[20] D. Morin, "The Lagrangian Method," in Computer Simulation of Shaped Charge Problems, 2006, pp. 5–30.

[21] Y. Mori, Easy-to-understand modern control theory [Japanese version]. Tokyo, Japan: Morikita Publishing Co. Ltd, 2013.

[22] S. O. H. Madgwick, "An efficient orientation filter for inertial and inertial/magnetic sensor arrays," 2010.

[23] A. Al-Fahoum and M. Abadir, "Design of a Modified Madgwick Filter for Quaternion-Based Orientation Estimation Using AHRS," Int. J. Comput. Electr. Eng., vol. 10, pp. 174–186, Oct. 2018, doi: 10.17706/IJCEE.2018.10.3.174-186.

[24] M. Hasan and M. H. Rahman, "Smart Phone Based Sensor Fusion by Using Madgwick Filter for 3D Indoor Navigation," Wirel. Pers. Commun., Apr. 2020, doi: 10.1007/s11277-020-07338-7.

APPENDICES

Appendix A: Equations of robot body coordinates and corresponding derivatives.

Wheel

$$\begin{bmatrix} x \\ y \end{bmatrix} = \begin{bmatrix} r(\varphi + \theta_1) \\ r \end{bmatrix}$$

$$\begin{bmatrix} \dot{x} \\ \dot{y} \end{bmatrix} = \begin{bmatrix} r(\dot{\varphi} + \dot{\theta}_1) \\ 0 \end{bmatrix}$$

Body 1

$$\begin{bmatrix} x \\ y \end{bmatrix} = \begin{bmatrix} r(\varphi + \theta_1) - l_1 \sin\theta_1 \\ r - l_1 \cos\theta_1 \end{bmatrix}$$

$$\begin{bmatrix} \dot{x} \\ \dot{y} \end{bmatrix} = \begin{bmatrix} r(\dot{\varphi} + \dot{\theta_1}) - l_1\dot{\theta_1} \cos\theta_1 \\ l_1\dot{\theta_1} \sin\theta_1 \end{bmatrix}$$

Body 2

$$\begin{bmatrix} x \\ y \end{bmatrix} = \begin{bmatrix} r(\varphi + \theta_1) + d\sin\theta_1 + l_2\sin(\theta_1 + \theta_2) \\ r + d\cos\theta_1 + l_2\cos(\theta_1 + \theta_2) \end{bmatrix}$$

$$\begin{bmatrix} \dot{x} \\ \dot{y} \end{bmatrix} = \begin{bmatrix} r(\dot{\varphi} + \dot{\theta}_1) + d\,\dot{\theta}_1\cos\theta_1 + l_2(\dot{\theta}_1 + \dot{\theta}_2)\cos(\theta_1 - \\ -d\dot{\theta}_1\sin\theta_1 - l_2(\dot{\theta}_1 + \dot{\theta}_2)\sin(\theta_1 + \theta_2) \end{bmatrix}$$

Body 3

$$\begin{bmatrix} x \\ y \end{bmatrix} = \begin{bmatrix} r(\varphi + \theta_1) + d\sin\theta_1 + L_2\sin(\theta_1 + \theta_2) + \cdots \\ r + d\cos\theta_1 + L_2\cos(\theta_1 + \theta_2) + \cdots \\ \cdots \quad l_3\sin(\theta_1 + \theta_2 + \theta_3) \\ \cdots \quad l_3\cos(\theta_1 + \theta_2 + \theta_3) \end{bmatrix}$$

$$\begin{bmatrix} \dot{x} \\ \dot{y} \end{bmatrix} = \begin{bmatrix} r(\dot{\varphi} + \dot{\theta}_1) + d\,\dot{\theta}_1\cos\theta_1 + L_2(\dot{\theta}_1 + \dot{\theta}_2)\cos(\theta_1 \\ -d\dot{\theta}_1\sin\theta_1 - L_2(\dot{\theta}_1 + \dot{\theta}_2)\sin(\theta_1 + \theta_2) \\ \cdots \quad l_3(\dot{\theta}_1 + \dot{\theta}_2 + \dot{\theta}_3)\cos(\theta_1 + \theta_2 + \theta_3) \\ \cdots \quad l_3(\dot{\theta}_1 + \dot{\theta}_2 + \dot{\theta}_3)\sin(\theta_1 + \theta_2 + \theta_3) \end{bmatrix}$$

Appendix B: Derivation for equation of motion

$$\begin{aligned}&\left(M_{p1}+M_{p2}+M_{p3}+M_c\right)r^2+M_{p1}l_1^2-2M_{p1}rl_1cos\,\theta_1\\&+M_{p2}d^2+M_{p2}rl_2cos\,(\theta_1+\theta_2)\\&+2M_{p2}rd\,cos\,\theta_1+M_{p2}dl_2cos\,\theta_2\\&+M_{p3}d^2+M_{p3}rL_2cos\,(\theta_1+\theta_2)\\&+M_{p3}rl_3cos\,(\theta_1+\theta_2+\theta_3)\\&+2M_{p3}rdcos\,\theta_1+M_{p3}dL_2cos\,\theta_2\\&+M_{p3}dl_3cos\,(\theta_2+\theta_3)+J_{p1}+J_c\}\ddot{\theta}_1\\&+\{M_{p2}l_2^2+M_{p2}rl_2cos\,(\theta_1+\theta_2)\\&+M_{p2}dl_2cos\,\theta_2+M_{p3}L_2^2\\&+M_{p3}rL_2cos\,(\theta_1+\theta_2)+M_{p3}L_2l_3cos\,\theta_3\\&+M_{p3}dL_2cos\,\theta_2+J_{p2}\left(\ddot{\theta}_1+\ddot{\theta}_2\right)+M_{p3}l_3^2\\&+M_{p3}rl_3cos\,(\theta_1+\theta_2+\theta_3)\\&+M_{p3}L_2l_3cos\,\theta_3+M_{p3}dl_3cos\,(\theta_2+\theta_3)\\&+J_{p3}\left(\ddot{\theta}_1+\ddot{\theta}_2+\ddot{\theta}_3\right)\\&+\left(M_{p1}+M_{p2}+M_{p3}+M_c\right)r^2\\&-M_{p1}rl_1cos\,\theta_1+M_{p2}rl_2cos\,(\theta_1+\theta_2)\\&+M_{p2}rdcos\,\theta_1+M_{p3}rL_2cos\,(\theta_1+\theta_2)\\&+M_{p3}rl_3cos\,(\theta_1+\theta_2+\theta_3)\\&+M_{p3}rdcos\,\theta_1+J_c\ddot{\varphi}+C_{p1}\dot{\theta}_1\\&+M_{p1}rl_1\dot{\theta}_1^2sin\,\theta_1\\&-M_{p2}rl_2\left(\dot{\theta}_1+\dot{\theta}_2\right)^2sin\,(\theta_1+\theta_2)\\&-M_{p2}rd\dot{\theta}_1^2sin\,\theta_1-M_{p2}dl_2\dot{\theta}_1\dot{\theta}_2sin\,\theta_2\\&-M_{p2}dl_2\left(\dot{\theta}_1+\dot{\theta}_2\right)\dot{\theta}_2sin\,\theta_2\\&-M_{p3}rL_2\left(\dot{\theta}_1+\dot{\theta}_2\right)^2sin\,(\theta_1+\theta_2)\\&-M_{p3}rl_3\left(\dot{\theta}_1+\dot{\theta}_2+\dot{\theta}_3\right)^2sin\,(\theta_1+\theta_2\\&+\theta_3)-M_{p3}L_2l_3\left(\dot{\theta}_1+\dot{\theta}_2+\dot{\theta}_3\right)\dot{\theta}_3sin\,\theta_3\\&-M_{p3}dL_2\dot{\theta}_1\dot{\theta}_2sin\,\theta_2\\&-M_{p3}dL_2\left(\dot{\theta}_1+\dot{\theta}_2\right)\dot{\theta}_2sin\,\theta_2\\&-M_{p3}dl_3\dot{\theta}_1\left(\dot{\theta}_2+\dot{\theta}_3\right)sin\,(\theta_2+\theta_3)\\&-M_{p3}dl_3\left(\dot{\theta}_1+\dot{\theta}_2+\dot{\theta}_3\right)\left(\dot{\theta}_2+\dot{\theta}_3\right)sin\,(\theta_2\\&+\theta_3)-M_{p3}rd\dot{\theta}_1^2sin\,\theta_1+M_{p1}gl_1sin\,\theta_1\\&-M_{p2}gdsin\,\theta_1-M_{p3}gdsin\,\theta_1\\&-M_{p2}gl_2sin\,(\theta_1+\theta_2)\\&-M_{p3}gL_2sin\,(\theta_1+\theta_2)-M_{p3}gl_3sin\,(\theta_1\\&+\theta_2+\theta_3)=0\end{aligned}\qquad(B1)$$

$$\begin{aligned}&M_{p2}rl_2cos\,(\theta_1+\theta_2)+M_{p2}dl_2cos\,\theta_2\\&+M_{p3}rL_2cos\,(\theta_1+\theta_2)\\&+M_{p3}rl_3cos\,(\theta_1+\theta_2+\theta_3)\\&+M_{p3}dL_2cos\,\theta_2\\&+M_{p3}dl_3cos\,(\theta_2+\theta_3)\,\ddot{\theta}_1\\&+\left\{M_{p2}l_2^2+M_{p3}L_2^2+M_{p3}L_2l_3cos\,\theta_3\right.\\&\left.+J_{p2}\right\}\left(\ddot{\theta}_1+\ddot{\theta}_2\right)\\&+\left\{M_{p3}l_3^2+M_{p3}L_2l_3cos\,\theta_3+J_{p3}\right\}\left(\ddot{\theta}_1+\ddot{\theta}_2\right.\\&\left.+\ddot{\theta}_3\right)\\&+\left\{M_{p2}rl_2cos\,(\theta_1+\theta_2)\right.\\&+M_{p3}rL_2cos\,(\theta_1+\theta_2)\\&\left.+M_{p3}rl_3cos\,(\theta_1+\theta_2+\theta_3)\right\}\ddot{\varphi}+C_{p2}\dot{\theta}_2\\&-M_{p3}L_2l_3\left(\dot{\theta}_1+\dot{\theta}_2+\dot{\theta}_3\right)\dot{\theta}_3sin\,\theta_3\\&-M_{p3}L_2l_3\left(\dot{\theta}_1+\dot{\theta}_2\right)\dot{\theta}_3sin\,\theta_3\\&-M_{p2}dl_2\dot{\theta}_1\dot{\theta}_2sin\,\theta_2\\&+M_{p2}dl_2\dot{\theta}_1\left(\dot{\theta}_1+\dot{\theta}_2\right)sin\,\theta_2\\&-M_{p3}dL_2\dot{\theta}_1\dot{\theta}_2sin\,\theta_2\\&-M_{p3}dl_3\dot{\theta}_1\left(\dot{\theta}_2+\dot{\theta}_3\right)sin\,(\theta_2+\theta_3)\\&+M_{p3}dL_2\dot{\theta}_1\left(\dot{\theta}_1+\dot{\theta}_2\right)sin\,\theta_2\\&+M_{p3}dl_3\dot{\theta}_1\left(\dot{\theta}_1+\dot{\theta}_2+\dot{\theta}_3\right)sin\,(\theta_2+\theta_3)\\&-M_{p2}gl_2sin\,(\theta_1+\theta_2)\\&-M_{p3}gL_2sin\,(\theta_1+\theta_2)-M_{p3}gl_3sin\,(\theta_1\\&+\theta_2+\theta_3)\\&=a_{p2}u_{p2}\end{aligned}\qquad(B2)$$

$$\begin{aligned}&M_{p3}rl_3cos\,(\theta_1+\theta_2+\theta_3)+M_{p3}dl_3cos\,(\theta_2+\theta_3)\,\ddot{\theta}_1\\&+\left\{M_{p3}L_2l_3cos\,\theta_3\right\}\left(\ddot{\theta}_1+\ddot{\theta}_2\right)\\&+\left\{M_{p3}l_3^2+J_{p3}\right\}\left(\ddot{\theta}_1+\ddot{\theta}_2+\ddot{\theta}_3\right)\\&+\left\{M_{p3}rl_3cos\,(\theta_1+\theta_2+\theta_3)\right\}\ddot{\varphi}+C_{p3}\dot{\theta}_3\\&-M_{p3}L_2l_3\left(\dot{\theta}_1+\dot{\theta}_2\right)\dot{\theta}_3sin\,\theta_3\\&+M_{p3}L_2l_3\left(\dot{\theta}_1+\dot{\theta}_2\right)\left(\dot{\theta}_1+\dot{\theta}_2+\dot{\theta}_3\right)sin\,\theta_3\\&-M_{p3}dl_3\dot{\theta}_1\left(\dot{\theta}_2+\dot{\theta}_3\right)sin\,(\theta_2+\theta_3)\\&+M_{p3}dl_3\dot{\theta}_1\left(\dot{\theta}_1+\dot{\theta}_2+\dot{\theta}_3\right)sin\,(\theta_2\\&+\theta_3)-M_{p3}gl_3sin\,(\theta_1+\theta_2+\theta_3)\\&=a_{p3}u_{p3}\end{aligned}\qquad(B3)$$

$$\begin{aligned}&\left\{\left(M_{p1}+M_{p2}+M_{p3}+M_c\right)r^2-M_{p1}rl_1cos\,\theta_1\right.\\&\left.+M_{p2}rdcos\,\theta_1+M_{p3}rdcos\,\theta_1+J_c\right\}\ddot{\theta}_1\\&+\left\{M_{p2}rl_2cos\,(\theta_1+\theta_2)\right.\\&\left.+M_{p3}rL_2cos\,(\theta_1+\theta_2)\right\}\left(\ddot{\theta}_1+\ddot{\theta}_2\right)\\&+\left\{M_{p3}rl_3cos\,(\theta_1+\theta_2+\theta_3)\right\}\left(\ddot{\theta}_1+\ddot{\theta}_2\right.\\&\left.+\ddot{\theta}_3\right)\\&+\left\{\left(M_{p1}+M_{p2}+M_{p3}+M_c\right)r^2+J_c\right\}\ddot{\varphi}\\&+C_c\dot{\varphi}+M_{p1}rl_1\dot{\theta}_1^2sin\,\theta_1\\&-M_{p2}rl_2\left(\dot{\theta}_1+\dot{\theta}_2\right)^2sin\,(\theta_1+\theta_2)\\&-M_{p2}rd\dot{\theta}_1^2sin\,\theta_1\\&-M_{p3}rL_2\left(\dot{\theta}_1+\dot{\theta}_2\right)^2sin\,(\theta_1+\theta_2)\\&-M_{p3}rl_3\left(\dot{\theta}_1+\dot{\theta}_2+\dot{\theta}_3\right)^2sin\,(\theta_1+\theta_2\\&+\theta_3)-M_{p3}rd\dot{\theta}_1^2sin\,\theta_1=a_cu_c\end{aligned}\qquad(B4)$$

https://doi.org/10.25077/jnte.v12n2.1106.2023

Appendix C: Derivation of linearized model equations

$$\begin{aligned}&\left(M_{p1}+M_{p2}+M_{p3}+M_c\right)r^2+M_{p1}l_1^2-2M_{p1}rl_1+M_{p2}d^2\\&\quad+M_{p2}rl_2+2M_{p2}rd+M_{p2}dl_2+M_{p3}d^2\\&\quad+M_{p3}rL_2+M_{p3}rl_3+2M_{p3}rd+M_{p3}dL_2\\&\quad+M_{p3}dl_3+J_{p1}+J_c\ddot{\theta}_1\\&\quad+\left\{M_{p2}l_2^2+M_{p2}rl_2+M_{p2}dl_2+M_{p3}L_2^2\right.\\&\quad\left.+M_{p3}rL_2+M_{p3}L_2l_3+M_{p3}dL_2+J_{p2}\right\}\left(\ddot{\theta}_1\right.\\&\quad\left.+\ddot{\theta}_2\right)\\&\quad+\left\{M_{p3}l_3^2+M_{p3}rl_3+M_{p3}L_2l_3+M_{p3}dl_3\right.\\&\quad\left.+J_{p3}\right\}\left(\ddot{\theta}_1+\ddot{\theta}_2+\ddot{\theta}_3\right)\\&\quad+\left\{\left(M_{p1}+M_{p2}+M_{p3}+M_c\right)r^2-M_{p1}rl_1\right.\\&\quad+M_{p2}rl_2+\left.M_{p2}rd+M_{p3}rL_2+M_{p3}rl_3\right.\\&\quad+\left.M_{p3}rd+J_c\right\}\ddot{\varphi}+C_{p1}\dot{\theta}_1\\&\quad+\left\{M_{p1}gl_1-M_{p2}gd-M_{p3}gd\right\}\theta_1\\&\quad-\left\{M_{p2}gl_2+M_{p3}gL_2\right\}(\theta_1\\&\quad+\theta_2)-M_{p3}gl_3(\theta_1+\theta_2+\theta_3)=0\qquad(C1)\end{aligned}$$

$$\begin{aligned}&\left\{M_{p2}rl_2+M_{p2}dl_2+M_{p3}rL_2+M_{p3}rl_3+M_{p3}dL_2\right.\\&\quad\left.+M_{p3}dl_3\right\}\ddot{\theta}_1\\&\quad+\left\{M_{p2}l_2^2+M_{p3}L_2^2+M_{p3}L_2l_3+J_{p2}\right\}\left(\ddot{\theta}_1\right.\\&\quad\left.+\ddot{\theta}_2\right)\\&\quad+\left\{M_{p3}l_3^2+M_{p3}L_2l_3+J_{p3}\right\}\left(\ddot{\theta}_1+\ddot{\theta}_2+\ddot{\theta}_3\right)\\&\quad+\left\{M_{p2}rl_2+M_{p3}rL_2+M_{p3}rl_3\right\}\ddot{\varphi}-C_{p2}\dot{\theta}_1\\&\quad+C_{p2}\left(\dot{\theta}_1+\dot{\theta}_2\right)\\&\quad-\left\{M_{p2}gl_2+M_{p3}gL_2\right\}(\theta_1\\&\quad+\theta_2)-M_{p3}gl_3(\theta_1+\theta_2+\theta_3)\\&\quad=a_{p2}u_{p2}\qquad(C2)\end{aligned}$$

$$\begin{aligned}&\left\{M_{p3}rl_3+M_{p3}dl_3\right\}\ddot{\theta}_1+M_{p3}L_2l_3\left(\ddot{\theta}_1+\ddot{\theta}_2\right)\\&\quad+\left\{M_{p3}l_3^2+J_{p3}\right\}\left(\ddot{\theta}_1+\ddot{\theta}_2+\ddot{\theta}_3\right)+M_{p3}rl_3\ddot{\varphi}\\&\quad-C_{p3}\left(\dot{\theta}_1+\dot{\theta}_2\right)\\&\quad+C_{p3}\left(\dot{\theta}_1+\dot{\theta}_2+\dot{\theta}_3\right)-M_{p3}gl_3(\theta_1+\theta_2\\&\quad+\theta_3)=a_{p3}u_{p3}\qquad(C3)\end{aligned}$$

$$\begin{aligned}&\left\{\left(M_{p1}+M_{p2}+M_{p3}+M_c\right)r^2-M_{p1}rl_1+M_{p2}rd+M_{p3}rd\right.\\&\quad\left.+J_c\right\}\ddot{\theta}_1+\left\{M_{p2}rl_2+M_{p3}rL_2\right\}\left(\ddot{\theta}_1+\ddot{\theta}_2\right)\\&\quad+M_{p3}rl_3\left(\ddot{\theta}_1+\ddot{\theta}_2+\ddot{\theta}_3\right)\\&\quad+\left\{\left(M_{p1}+M_{p2}+M_{p3}+M_c\right)r^2+J_c\right\}\ddot{\varphi}\\&\quad=a_cu_c\qquad(C4)\end{aligned}$$